JOURNAL OF MATERIALS SCIENCE **33** (1998) 5059–5067

Capillary flow behaviour of microcrystalline wax and silicon carbide suspension

H. SUWARDIE, R. YAZICI, D. M. KALYON*, S. KOVENKLIOGLU
Highly Filled Materials Institute, Chemical Sciences and Engineering, Stevens Institute of Technology, Castle Point on Hudson, Hoboken, NJ 07030, USA

Suspensions of ceramic particles in low or high molecular weight polymers are shaped into various three-dimensional parts using various moulding and extrusion technologies. Such bodies are subsequently fired-up and sintered to remove the binder. The utilities of such three-dimensional ceramic bodies depend on the restrictions related to the shapeability of the ceramic suspension, hence to the flow and deformation behaviour of the suspension. In this study, factors affecting the flow and deformation behaviour of a 50% by volume of silicon carbide in a wax binder was investigated. Consistent with the previously observed behaviour of other highly filled materials, the ceramic suspension exhibited viscoplasticity, plug flow and wall slip. Furthermore, flow instabilities associated with the axial migration of the low viscosity binder under the imposed pressure gradient were observed. These results pinpoint to the various difficulties associated with the collection of rheological data and emphasize the relevance of various flow mechanisms, including wall slip and mat formation and filtration based flow instabilities, which would also occur in processing/shaping flows of such ceramic suspensions including extrusion and moulding.

1. Introduction

Numerous industrial applications involve the shaping of ceramic suspensions using various processing including extrusion and injection moulding. In such processing, fine ceramic powder is mixed with a blend of polymers, hydrogels or waxes and processing aids/surfactants to impart fluidity so that the suspensions can be processed and shaped into a desired shape. The polymeric binder is subsequently removed before the sintering of the shaped article. Other processing techniques include colloidal processing of nanoparticles, sol–gel methods and the organometallic route [1–4]. In organometallic processing, the thermal behaviour and processability of the organometallic polymer precursor is critical [5, 6] and the formation of the pores during pyrolysis of the polymer requires special attention [7].

In the shaping of the ceramic green bodies via extrusion or moulding, the processability of the ceramic suspension needs to be characterized. Such characterization generally involves subjecting the ceramic suspension to a series of viscometric flow experiments which allow the rheological material functions of the suspension to be characterized. Various factors involved in the rheological behaviour of concentrated suspensions are reviewed by others [8–14]. The existing literature on the experimental and theoretical work on dilute and concentrated suspensions generally emphasize the effects of shape, size distribution and volume fraction of particles, particle–particle and particle–matrix interactions and the rheological behaviour of the matrix as the principal contributors to the complex flow behaviour of suspensions.

However, the ceramic suspensions used in various extrusion and moulding applications are generally filled with solids at loading levels which approach the maximum packing fraction. The rheological characteristics of such highly filled materials are significantly affected by wall slip [9, 15–17], development of flow instabilities during capillary and slit flows associated with the axial migration of the matrix under the imposed pressure gradient [18, 19], and dilatancy [10, 20]. Furthermore, the entrainment of air into the suspensions occurs at the partially full sections of the processors [21], especially where the ingredients of the ceramic suspensions are compounded together. Kalyon *et al*. [22] and Aral and Kalyon [23] have shown that the air entrained during processing alters the rheological behaviour, including the apparent wall slip layer formation during suspension flow [24]. When the particle radius is sufficiently large in comparison to the channel dimension, particle migration effects associated with the shear rate and concentration gradients are also expected to play a role [25–31]. The characterization of such effects including wall slip, flow instabilities, particle migration, air entrainment, etc., are labour intensive and difficult and were generally omitted from the characterization of the rheological behaviour of ceramic suspensions [32–34].

* Author for correspondence.

The wall slip effect was investigated by Isayev [35] by the use of knurled and smooth rheometer surfaces. Significant wall slip was observed. However, the use of grooved surfaces is generally not sufficient to eliminate wall slip. This is because the use of grooved surfaces can still give rise to slip at the tip of the grooves and/or fracture the suspension sample [17].

In this paper we summarize some of our findings related to the capillary flow behaviour of a ceramic suspension involving 50% by volume of SiC particles incorporated into a wax/stearic acid binder. Various factors including wall slip and flow instabilities were investigated as part of this rheological characterization study.

2. Experimental procedure

2.1. Materials

The scanning electron micrograph and particle size distribution of the SiC powder used in this study is shown in Fig. 1a and b, respectively. The SiC powder (77.6% by weight) was compounded with 2.5% by weight of stearic acid and 19.9% by weight of wax. The SiC was available from Superior Graphite (Chicago, IL), the stearic acid from Fisher Scientific USA and the microcrystalline wax from Frank Ross Wax (New Jersey). The corresponding volume concentrations are shown in Table I. The maximum packing fraction of SiC powder was calculated to be 0.672 [36].

From its molecular structure the shear viscosity of the binder (stearic acid and wax) was estimated to be smaller than 0.01 Pa s for the temperature range of 95 to 175 °C [36]. The shear viscosity of the wax was also experimentally characterized first by using capillary flow in conjunction with Instron capillary rheometer. The

TABLE I The composition, i.e. percent weight and percent volume of the components of the suspension used in the experiments

	SiC suspension (50 vol %)	
	(wt %)	(vol %)
SiC HSC-059	77.56	50.00
Microwax	19.94	44.54
Stearic acid	2.50	5.46
Total	100.00	100.00

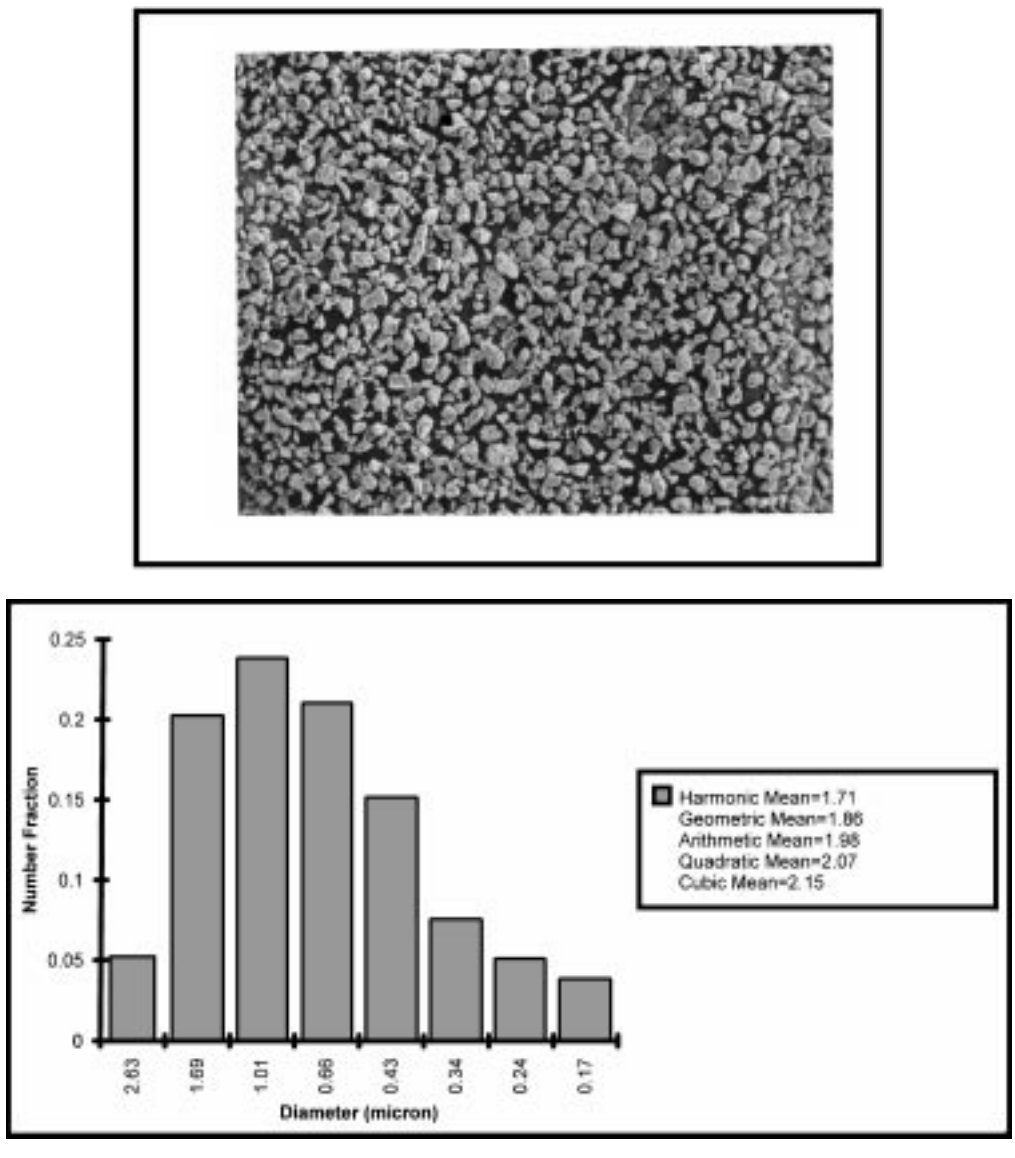

Figure 1 (a) Scanning electron micrograph of SiC HSC-059 (1000× magnification). (b) Particle size distribution of silicon carbide powder.

capillary flow experiments were carried out at the relatively high shear rate range by using a capillary with a diameter of 0.3 mm. The shear viscosity of the wax at 175 °C was around 3.8×10^{-3} Pa s. However, significant viscous energy dissipation occurs at such high deformation rates resulting at higher temperatures at the wall. These non-isothermal effects were not corrected for in these experiments. A second set of experiments with a constant stress rheometer was carried-out under well-controlled temperature conditions.

A Rheometric Scientific Dynamic Stress Rheometer, SR-200 was used in conjunction with the Heated Plates Environmental System. Parallel discs with 40 mm diameter were employed. The gap separation was kept around 0.5 ± 0.02 mm. The steady shear viscosity values of the wax were obtained by steady shear stress sweep tests. In these tests the shear stress at the edge was varied. At each shear stress the sample was allowed up to a 60 s time period to reach the steady state in shear rate, which was determined using the Automatic Steady State Sensing Option of the SR-200.

The steady shear viscosity values of the binder obtained using both methods at 175 °C are shown in Fig. 2. The shear viscosity values are presented as 95% confidence intervals determined according to Student's

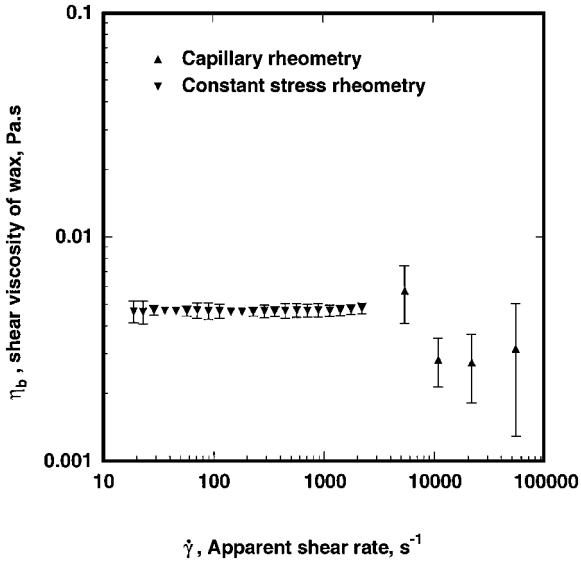

Figure 2 Shear viscosity of the wax based binder as a function of wall shear rate at $T = 175\,^{\circ}$C.

t-distribution. Fig. 2 indicates that the wax based binder behaves like a Newtonian fluid over the broad shear rate range of 20–4000 s^{-1}. The mean value of steady shear viscosity values obtained with rotational rheometry at 175 °C is 4.5×10^{-3} Pa s. This value is slightly higher than the mean value of 3.8×10^{-3} Pa s obtained from capillary rheometry.

2.2. Compounding

The ceramic suspension samples were compounded in a Haake Torque Rheometer with a 60 cm^3 mixing volume at 175 °C. The mixing was carried-out in two steps where first the binder (microcrystalline wax and stearic acid) was mixed followed by the addition of the solid phase. Eighty percent of the available volume of the mixer was used. The specific energy input, E_s, during mixing was determined from the following

$$E_s = \frac{2\pi N}{m} \int M \, dt \qquad (1)$$

where: E_s is specific energy input, i.e. mechanical energy which the mixer rotors dissipate into the sample (J g^{-1}); N is rotational speed of the agitator blades; m is mass of the sample (g); $\int M \, dt$ is integrated torque.

Fig. 3 shows the comparison of the specific energy input for compounding for two volume fractions of SiC, i.e. $\phi = 0.5$ and 0.6. As the volume loading level of solids, ϕ, increases and approaches the maximum packing fraction, the shear viscosity and hence the specific energy input during compounding increases significantly. The specific energy input was reproducible and was used as a parameter for consistent preparation of suspension samples used in rheological characterization.

2.3. Microscopy

A Jeol-850 scanning electron microscope (SEM) with 50 nm resolution and energy dispersive X-Ray analysis (EDX) were utilized as the principal tools for the microstructural analysis of the batch mixed and extruded green grains.

The degree of mixing of the wax binder and the SiC particles was analysed at the fractured cross-section of

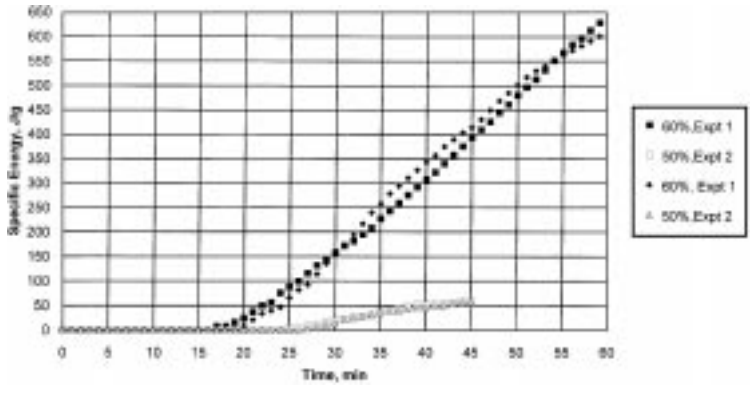

Figure 3 Specific energy input during compounding of 50% and 60% (by volume) of SiC with wax based binder.

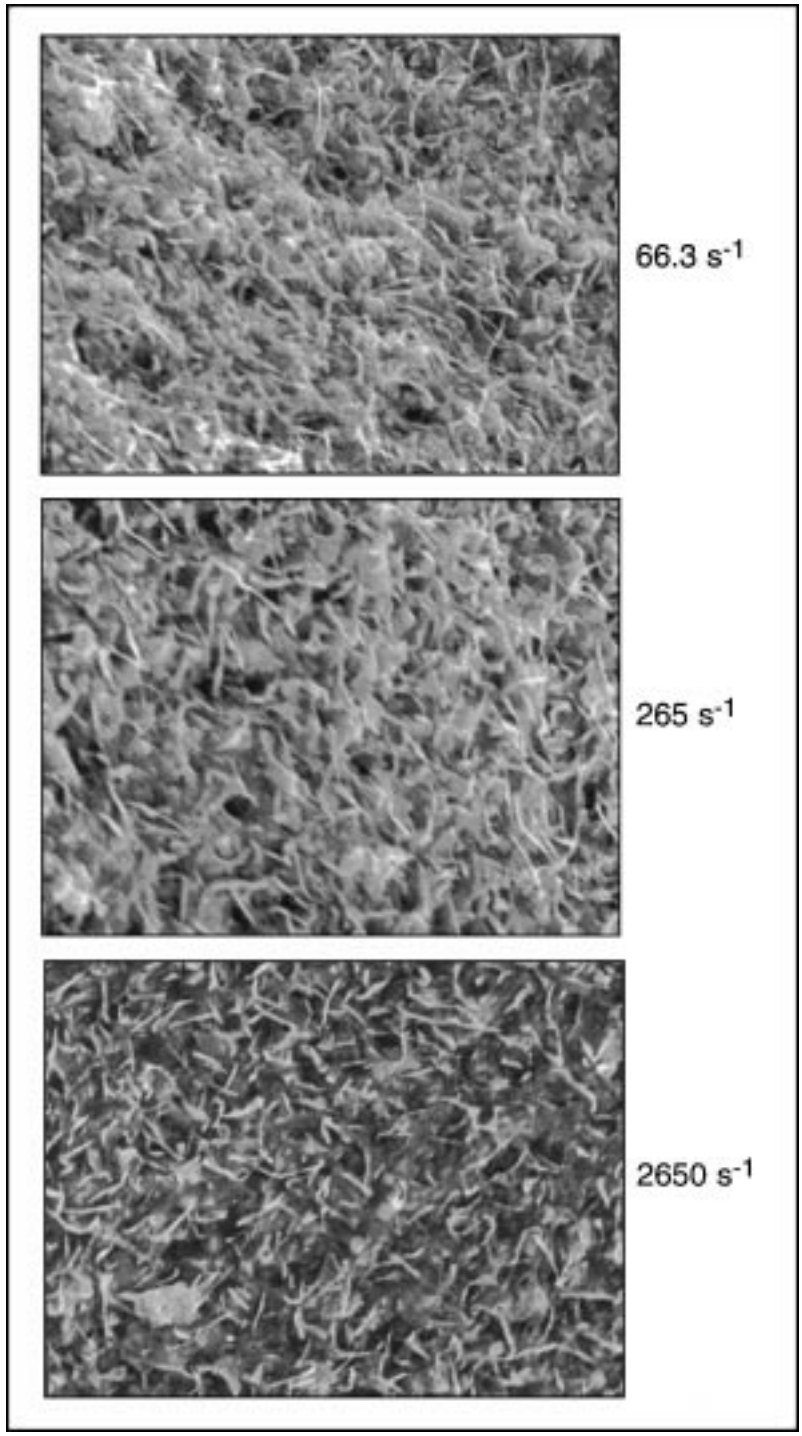

Figure 4 Scanning electron micrographs of extruded ceramic suspension sample at 3000× magnification.

the shaped samples. The typical SEM micrographs of the fractured cross-sections are shown in Fig. 4. Fig. 4 shows that upon fracturing, the binder goes through a ductile type deformation and protrudes from between SiC particles as thin sheets on the fractured surface.

The mean distance between these protruded binder layers is approximately 2 μm or about twice the number-based average diameter of SiC particles. These features provide direct evidence that establishes the upper limit of the agglomeration of SiC particles. They suggest that the degree of mixing is inadequate at a scale that is less than 2 μm. However, at larger scales, the degree of mixing was acceptable. This figure also indicates that the thickness of the binder layer is about 0.15 μm, indicating good wetting and good intermixing of the binder and the SiC particles.

2.4. Capillary rheometry of the suspension

The ceramic suspension samples, compounded in the batch mixer, were characterized employing capillary and parallel disk torsional flows at 175 °C. For capillary flow experiments, an Instron capillary rheometer, Model FTD, was employed in conjunction with three sets of capillaries. Each set contained four capillaries. The capillaries had diameters of 1.3, 1.6 and 2 mm and

length/diameter ratios of 0, 19.2, 38.4 and 57.6. The data were collected by repeating the experiment at least three times per run, followed by statistical analysis.

The apparent shear stress versus the apparent shear rate, $\dot{\gamma}_a$, data were determined from the raw data (plunger force versus cross head speed) using

$$\dot{\gamma}_{\mathrm{a}} = \frac{32Q}{\pi D^3} \tag{2}$$

where D is diameter of capillary and Q is the volumetric flow rate. The volumetric flow rate, Q, is equal to the product of $\bar{V}$ (cross-head speed of the plunger) and cross-sectional area of the barrel of the rheometer. The apparent shear stress, $\tau_{\mathrm{w,a}}$ at the wall is given by

$$\tau_{\mathrm{w,a}} = \frac{\Delta P}{4L/D} \tag{3}$$

The true shear stress at the wall, τ_{w}, needs to be determined by correcting for the pressure drop associated with the end effects [37]. Thus Equation 3 is modified to

$$\tau_{\mathrm{w}} = \frac{\Delta P D}{4(L + ND)} \tag{4}$$

where ΔP is total pressure drop, L is the length of the capillary and N is equivalent length associated with the end corrections. The equivalent length can be determined by the extrapolation of the pressure drop versus the L/D ratio curve at constant apparent shear rate to intersect the L/D axis.

To determine the slip effects, capillaries with the same L/D ratio but with different diameters were used. Analysis of the fully developed, incompressible, isothermal and laminar flow in circular tubes with a slip velocity of u_{s}, at the wall yields [38]

$$\frac{8\bar{V}}{D} = \frac{4}{\tau_{\mathrm{w}}^3}\int_0^{\tau_{\mathrm{w}}} \tau^2\dot{\gamma}\,\mathrm{d}\tau + \frac{8u_{\mathrm{s}}}{D} \tag{5}$$

where τ is the shear stress and $\dot{\gamma}$ is the true shear rate.

Differentiating the last equation with respect to $1/D$ at constant shear stress at the wall, τ_{w}, one obtains

$$\left.\frac{\partial(8\bar{V}/D)}{\partial(1/D)}\right|_{\tau_{\mathrm{w}}} = 8u_{\mathrm{s}} \tag{6}$$

Thus, the plot of the apparent shear rate, $(8\bar{V}/D) = \dot{\gamma}_{\mathrm{a}}$ versus $1/D$ at constant shear stress τ_{w} should give rise to a straight line with a slope of $8u_{\mathrm{s}}$. The contribution of the slip to the total volumetric flow rate, Q_{s}, can be determined as follows

$$Q_{\mathrm{s}} = (\pi/4)D^2u_{\mathrm{s}} \tag{7}$$

Thus, the ratio of flow due to slip, Q_{s}, over the total flow rate, Q, is given as

$$(Q_{\mathrm{s}}/Q) = (u_{\mathrm{s}}/\bar{V}) = (8u_{\mathrm{s}}/D\dot{\gamma}_{\mathrm{a}}) \tag{8}$$

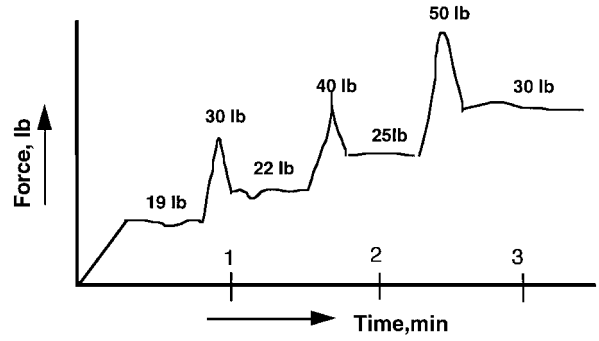

Figure 5 Time-dependent plunger force encountered during capillary flow for a capillary with a length diameter ratio of 57.6 and diameter of 1.32 mm at an apparent shear rate of 67 s^{-1} at 175 °C.

3. Results and discussion

Up to a cross-head speed of 0.85 mm s^{-1} for all the capillaries, (apparent shear rate of less than 140 s^{-1}), the wall shear stress consistently exhibited significant time-dependent variations. These fluctuations over the course of capillary flow were greatly diminished at the higher apparent shear rates. A typical plunger force versus time plot as collected at an apparent shear rate of 66 s^{-1} is shown in Fig. 5. The plunger force increases with increasing extrusion time and grows in an unbounded fashion. At regular intervals, stress overshoots are observed. This type of unstable behaviour was observed at the relatively low deformation rates. Unstable flows generally occur on the basis of the formation of a mat of solids at the converging section of the die and the concomitant filtration of the binder [18, 19]. Kalyon and co-workers have determined that under such unstable flow conditions the average pressure necessary to extrude the concentrated suspension grows unbounded with time. The oscillations in pressure are related to the time periodic mechanism of the formation of a mat of solids at the entrance of the capillary die and the time-dependent filtration of the binder. The declining concentration of the binder in the reservoir with time in turn increases the overall pressure drop necessary to extrude the suspension out of the capillary. In general, such flow instabilities can be eliminated by increasing the viscosity of the matrix (for example by lowering of the temperature), increasing the shear stress at the wall and by using dies with greater diameter [18, 19].

For all capillaries used in the experiments, the flow instabilities occurred at apparent shear rates less than 140 s^{-1}. Yilmazer *et al.* [18] and Yaras *et al.* [19] have analysed such flow instabilities by considering the analogy of the flow of Generalized Newtonian fluids through a packed bed. From their analysis, the critical apparent shear rate below which the flow instabilities occur, can be determined.

This critical shear rate is determined from the comparison of the bulk velocity values with the filtration velocity of the binder. Flow instabilities associated with the filtration mechanism become predominant when the filtration velocity is comparable to the bulk velocity of the suspension flowing in the capillary. Although the mechanism of such flow instabilities were known

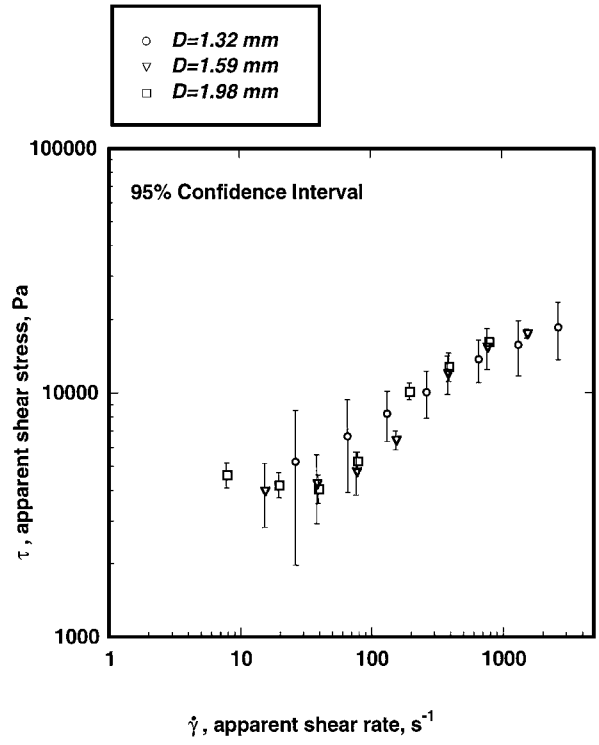

Figure 6 Apparent wall shear stress vs. apparent shear rate of 50 vol. % SiC suspension at 175 °C and capillary length/diameter ratio of 57.6.

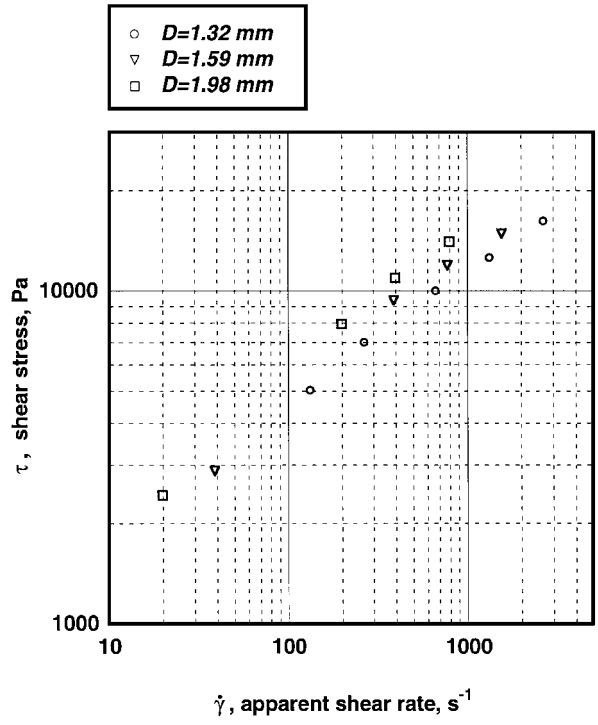

Figure 7 Corrected wall shear stress vs. apparent shear rate for 50 vol. % ceramic suspension at 175 °C and capillary length/diameter ratio of 57.6.

for some highly filled suspensions [18, 19], this is the first demonstration of this effect for ceramic suspensions. The occurrence of filtration based flow instabilities necessitate that capillary flow data be collected only for one shear rate at each filling of the barrel. Such demixing of the binder and the solid phase is also expected to occur during the extrusion or injection molding of such ceramic suspensions, especially when significant reductions in channel cross-sectional area are present.

The mean values of pressure drop were obtained for each shear rate from the time-dependent pressure drop data by using only the data collected during the first few minutes of each run. This was done in spite of the known limitations of averaging when flow instabilities are present. Fig. 6 shows the relationship between apparent shear stress and apparent shear rate for three capillaries with differing diameters but with a constant length/diameter, L/D, ratio of 57.6 and at 175 °C. The error bars were determined using 95% confidence interval, determined according to Students's t-distribution.

Fig. 7 shows the wall shear stress, corrected for end effects, as a function of apparent shear rate for the data reported in Fig. 6. With the exception of the shear rates smaller than 100 s^{-1}, the shear stress decreases with decreasing capillary diameter (increasing surface to volume ratio of the die). This behaviour is a typical precursor of wall slip [15]. As the surface to volume ratio increases (proportional to reciprocal diameter), the effect of wall slip becomes more pronounced; thus reducing the pressure drop through the capillary with decreasing capillary diameter at constant length/diameter ratio.

Assuming that the wall slip occurs on the basis of the formation of a lubrication layer, i.e. pure Newtonian binder layer at the wall, the shear rate at this slip layer can be calculated using the following [15]

$$\dot{\gamma}_{w,b}|_{\tau_w} = \frac{\tau_w}{\eta_b} \tag{9}$$

where η_b is the viscosity of the Newtonian binder and $\dot{\gamma}_{w,b}$ is the shear rate prevailing in the binder-rich apparent-slip region. For relatively small slip layer thickness the slip velocity at the wall can be determined from [15]

$$\dot{\gamma}_{w,b} = \frac{u_s}{\delta} \tag{10}$$

where u_s is the slip velocity at the wall and δ is the slip layer thickness. Previous findings of Kalyon and coworkers provide some guidance to how the slip layer thickness can be determined [39]. For example δ may be linked to the harmonic mean diameter, D_p, of the particles of the suspension

$$\delta = \frac{D_p}{8} \tag{11}$$

From the particle size distribution of silicon carbide particles presented in Fig. 1b, the harmonic mean particle diameter, D_p, of the ceramic particles was obtained

$$\text{Harmonic mean} = \left(\sum_j \frac{1}{D_j} V_j \right)^{-1} \tag{12}$$

where V_j is the volume fraction of particle j with diameter D_j. The harmonic mean diameter of silicon carbide particles was 1.7 μm. Hence, the slip layer thickness according to Equation 11 is around 0.2 μm.

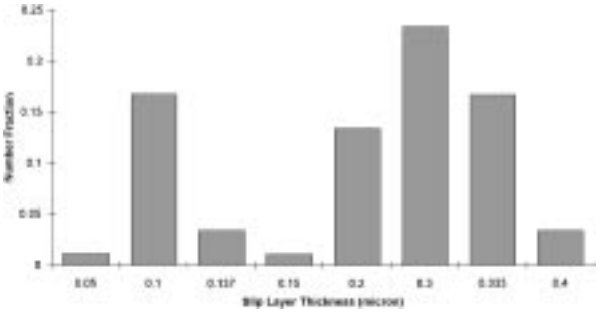

Figure 8 Slip layer thicknesses of extrudates of ceramic suspension as determined from scanning electron microscopy.

A correlation of δ/D_p versus ϕ/ϕ_m was developed by Yaras and Kalyon [39]. The data exhibited a linear behaviour between the slip layer thickness, δ, over the mean particle diameter, D_p, i.e. δ/D_p ratio, versus the volume percent of the particles, ϕ, over the maximum packing fraction of the particles, ϕ_m, i.e. ϕ/ϕ_m. This correlation which included data from multiple suspensions predicted a slip layer thickness of about 0.2 μm for the ceramic suspension of this study.

Using a third analysis technique, the slip layer thickness was also determined directly from the scanning electron micrographs of samples extruded during the capillary flow experiments. The apparent slip layer could be discerned with SEM as distinct binder layers on the surfaces of the as-extruded samples. At relatively high magnifications, edge-on measurements were carried-out on those regions of the surface slip layers which were partially detached and bent upon exit from the die. EDX analysis further confirmed the absence of SiC in these layers. These measurements were thus used to determine the thickness of the apparent layer thickness in various extruded grains. The distribution of the slip layer thickness values determined using SEM and EDX are shown in Fig. 8. This distribution has a mean thickness value of 0.22 μm which agrees with the apparent slip layer thickness value, i.e. 0.2 μm determined from using Equation 11 and the correlation reported in [39].

The slip velocity as a function of wall shear stress behaviour determined with two methods are shown in Fig. 9. The wall slip velocity increases with increasing wall shear stress. Such wall slip behaviour of concentrated suspensions are known to significantly affect their processability in various extrusion [40–42] and moulding flows. From the slip velocity, u_s, values, the ratio Q_s/Q, i.e. the volumetric flow rate due to slip over the total volumetric flow rate could be calculated using Equation 8. It was found that all Q_s/Q values calculated using Equation 8 were consistently equal to or greater than one, which indicated that the nature of the flow in the fully developed flow section of the capillary was plug flow. Obviously, values greater than one are not realistic but the consistent trend was the formation of plug flow lubricated at the wall, with an apparent slip layer consisting of the binder. Such plug flows were observed during the rheological characterization of various other highly filled materials also [15, 16].

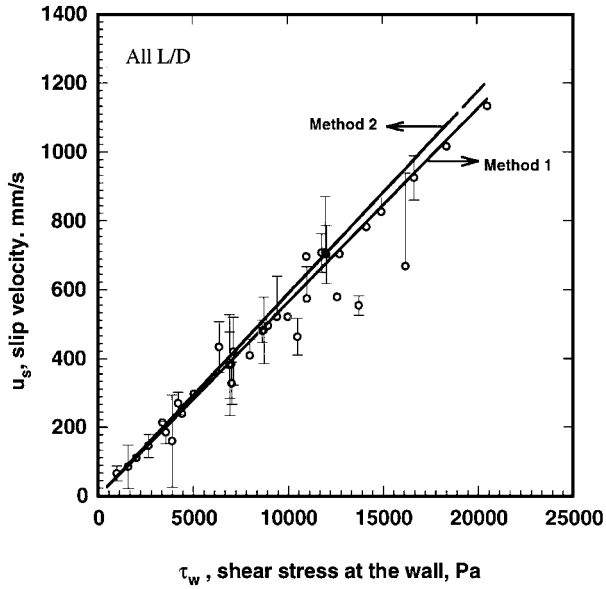

Figure 9 Slip velocity as a function of wall shear stress for 50 vol. % ceramic suspension at 175 °C.

The slip velocity values were determined also using the Mooney analysis method outlined in Equations 5–8. Mooney analysis also generates Q_s/Q values which are equal to or greater than one corroborating again that the ceramic suspension flows as a plug lubricated at the wall. Furthermore, attempts to characterize the ceramic suspension using rotational rheometry also gave rise to wall slip and concomitant plug-like flow of the suspension during steady torsional flow.

Because wall slip was determined to play such a key role the surfaces of the extrudates were analysed. The effect of capillary diameter on surface roughness of the extrudate is shown in Fig. 10. The capillaries had the same length over diameter ratio but differed in their diameters. These results suggest that the smallest diameter (1.32 mm) gives rise to the greatest surface roughness values for all three extrusion rates. The surfaces of the extrudates extruded at the highest extrusion rate are considerably rougher than those extruded at smaller cross-head speeds. These results again attest to the importance of surface phenomena in controlling the extrusion behaviour of such ceramic suspensions and the role played by the surface to volume ratio of the die used in extrusion process.

4. Conclusions

The capillary flow behaviour of a simple ceramic suspension consisting of a wax/stearic acid binder and 50% by volume of SiC particles was investigated employing capillaries with systematically varied diameters and length/diameter ratios. The capillary flow experiments revealed that this ceramic suspension generally flows as a plug lubricated at the wall by the formation of a binder-rich apparent slip layer. The thickness of the apparent slip layer was determined to be in the range of 0.17 to 0.22 μm. The plug flow of the ceramic suspension occurs concomitantly with the axial filtration of the low viscosity binder which is superimposed on the bulk flow of the suspension. These results indicate the

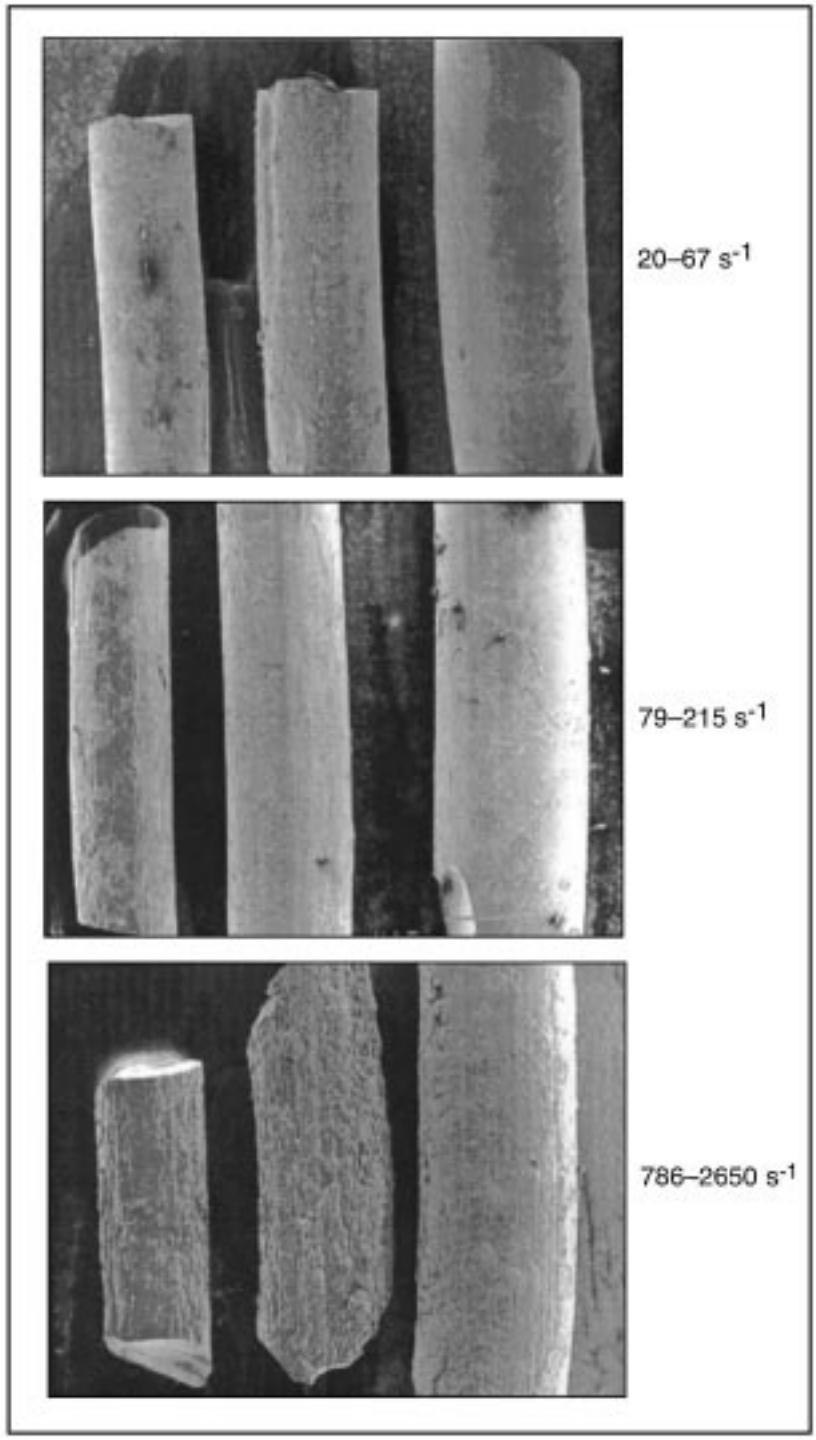

Figure 10 Scanning electron micrographs of surfaces of ceramic suspension samples extruded from capillaries with diameters of 1.32, 1.59 and 1.98 mm (15× magnification).

difficulties associated with the rheological characterization of concentrated suspensions of ceramic particles and the precautions which are necessary. Furthermore, various phenomena reported here including filtration based flow instabilities, wall slip and viscoplasticity should also prevail at various processing flows such as the extrusion [40–43] and injection moulding of such suspensions.

Acknowledgements

The shear viscosity of the binder was characterized using the constant stress rheometer by Dr B. Aral of Rheometric Scientific. We are grateful for the input of Dr P. Yaras, Dr B. Aral, and Dr T. Fiske and Dr A. Wagner on various aspects of the reported results.

References

1. L. HENCH and D. ULRICH, "Ultrastructure processing of ceramics, glass and composites" (John Wiley & Sons, New York, 1984).
2. *Idem.*, "Science of ceramic chemical processing" (John Wiley & Sons, New York, 1986).
3. Y. HASEGAWA, M. IIMURA and S. YAJIMA, *J. Mater. Sci.* **15** (1980) 720.
4. S. YAJIMA, *Amer. Ceram. Soc. Bull.* **62** (1983) 893.

5. D. M. KALYON and S. KOVENKLIOGLU, *Adv. Polym. Tech.* **7** (1987) 191.
6. H. SUWARDIE, D. M. KALYON and S. KOVENKLIOGLU, *J. Appl. Polym. Sci.* **42** (1991) 1087.
7. H. YAO, S. KOVENKLIOGLU and D. M. KALYON, *Chem. Eng. Commun.* **96** (1990) 155.
8. D. J. JEFFREY and A. ACRIVOS, *AlChE. J.* **22** (1976) 417.
9. H. A. BARNES, *J. Non-Newtonian Fluid Mech.* **56** (1995) 221.
10. R. L. HOFFMAN, *Adv. Coll. Interf. Sci.* **17** (1982) 161.
11. A. B. METZNER, *J. Rheol.* **29** (1985) 739.
12. M. R. KAMAL and A. MUTEL, *J. Polym. Eng.* **5** (1985) 293.
13. S. A. KHAN and R. K. PRUD'HOMME, *Rev. Chem. Eng.* **3** (1987) 205.
14. B. K. ARAL and D. M. KALYON, *J. Rheol.* **41** (1997) 599.
15. U. YILMAZER and D. M. KALYON, *J. Rheol.* **33** (1989) 1197.
16. D. M. KALYON, P. YARAS, B. ARAL and U. YILMAZER, *ibid.* **37** (1993) 35.
17. B. K. ARAL and D. M. KALYON, *ibid.* **38** (1994).
18. U. YILMAZER, C. G. GOGOS and D. M. KALYON, *Polym. Comp.* **10** (1989) 242.
19. P. YARAS, D. M. KALYON and U. YILMAZER, *Rheol. Acta* **33** (1994) 48.
20. U. YILMAZER and D. M. KALYON, *Polym. Comp.* **12** (1991) 226.
21. D. M. KALYON, C. JACOB and P. YARAS, *Plast. Rubber Comp. Proc. Appl.* **16** (1991) 193.
22. D. M. KALYON, R. YAZICI, C. JACOB, B. ARAL and S. SINTON, *Polym. Eng. Sci.* **31** (1991) 1386.
23. B. K. ARAL and D. M. KALYON, *Plast. Rubber Comp. Proc. Appl.* **24** (1995) 201.
24. D. M. KALYON, H. GOKTÜRK, P. YARAS and B. ARAL, *SPE ANTEC Tech. Papers* **41** (1995) 1130.
25. F. GADALA-MARIA and A. ACRIVOS, *J. Rheol.* **24** (1980) 799.
26. D. LEIGHTON and A. ACRIVOS, *J. Fluid Mech.* **275** (1994) 157.
27. A. KARNIS, H. L. GOLDSMITH and S. G. MASON, *Nature* **200** (1963) 159.
28. P. NOTT and J. BRADY, *J. Fluid. Mech.* **275** (1994) 157.
29. A. W. CHOW, S. W. SINTON, J. H. IWAMIYA and T. S. STEPHENS, *Phys. Fluids* **6** (1994) 2561.
30. R. PHILLIPS, R. C. ARMSTRONG, R. BROWN, A. L. GRAHAM and J. ABBOTT, *Phys. Fluids. A* **4** (1992) 30.
31. S. C. JANA, B. KAPOOR and A. ACRIVOS, *J. Rheol.* **39** (1995) 1123.
32. D. DORAISWAMY, I. L. TSAO, S. C. DANFORTH, A. N. BERIS and A. B. METZNER, in Proceedings of Xth International Congress on Rheology, (1988).
33. R. RAJKUMAR, PhD Thesis, State University of New York at Buffalo, 1991.
34. T. J. WHALEN, NASA Contractor Report #180831 (1989).
35. A. I. ISAYEV, "Advances in ceramics," vol. 21 (American Ceramic Society, Columbus, Ohio, 1987).
36. J. H. SUWARDIE, PhD Thesis, Stevens Institute of Technology, 1996.
37. E. B. BAGLEY, *J. Appl. Phys.* **28** (1957) 624.
38. M. MOONEY, *J. Coll. Sci.* **6** (1951) 162.
39. P. YARAS, PhD Thesis, Stevens Institute of Technology, 1995.
40. A. LAWAL, S. RAILKAR and D. KALYON, *J. Mater. Proc. Manuf. Sci.* **5** (1996) 57.
41. A. LAWAL and D. M. KALYON, *Int. J. Heat Mass Transfer* **40** (1997) 3883.
42. A. LAWAL and D. M. KALYON, *Num. Heat Transfer* **26** (1994) 103.
43. *Idem.*, *Polym. Eng. Sci.* **34** (1994) 1471.

Received 6 March
and accepted 22 July 1998